Chapter 6

New droplet structure and pattern formation in a polymer doped nematic liquid crystal

6.1 Introduction

Nematic drops nucleating from the isotropic phase, or dispersed in another isotropic liquid which is immiscible with the liquid crystal, show a variety of defect configurations [20, 68, 69, 70]. In such drops the director has a preferred orientation at the nematic–isotropic (NI) interface, for which the interfacial energy is a minimum. For a drop of size R, the interfacial energy is $\sim \gamma R^2$, where γ is the interfacial tension. Satisfying the boundary alignment condition will necessarily involve distortions of the director field inside the drop which costs an energy $\sim (K/R^2)R^3$, where K is the elastic constant of the nematic (see Sec. 1.2, Eq. 1.9). Equating the two energies gives a critical radius $R_c \sim K/\gamma$ beyond which it is favourable to distort the director field in order to satisfy the alignment condition. For the typical values, $K \sim 10^{-6}$ and $\gamma \sim 10^{-2}$, $R_c \sim 1\mu m$. Satisfying the alignment condition on such a closed surface necessarily involves the formation of topological defects called disclinations (see Sec.1.2). The types and configurations of these defects will depend on the elastic properties of the nematic apart from the alignment condition at the boundaries.

The Frank elastic free energy density for the director distortions in a nematic

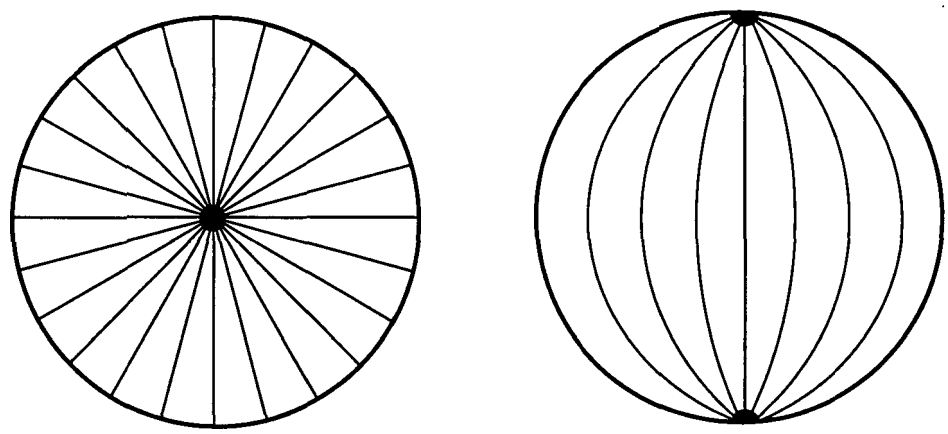

Figure 6.1: Schematic diagrams of the two commonly seen drop structures in nematic~.(a) the 'Hedge hog' structure forms when the preferred orientation of the director is normal to the interface. (b) the 'bipolar' structure occurs for tangential interfacial alignment.

---

medium is given by

$$f_N = \frac{1}{2}\left[K_{11}(\boldsymbol{\nabla}\cdot\hat{\mathbf{n}})^2 + K_{22}(\hat{\mathbf{n}}\cdot\boldsymbol{\nabla}\times\hat{\mathbf{n}})^2 + K_{33}(\hat{\mathbf{n}}\times\boldsymbol{\nabla}\times\hat{\mathbf{n}})^2\right] , \qquad (6.1)$$

where K_{11}, K_{22} and K_{33} are the elastic constants corresponding to splay, twist and bend deformations, respectively. For most nematics made of rod-like molecules, K22 $< K_{11} < K_{33}$.

The most commonly seen structures are the so called 'Hedge hog' (Fig. 6.1a) in the case of normal boundary alignment and the 'Bipolar' structure (Fig. 6.1b) in the case of tangential alignment condition [2].

In all the bipolar structures reported so far, the two disclinations occur diametrically opposite to each other. In this chapter, we describe studies conducted on a nematic liquid crystal doped with a polymeric material. The nematic droplets nucleating from the isotropic phase of such a mixture exhibit bipolar structures. As the drop size becomes large compared to the cell thickness, they become squashed between the two glass plates of the cell. In these 'disc-shaped' drops, the two point defects are no longer diametrically opposite to each other. Instead, they oc-

curred closer together along the edge of the disc. Moreover, large nematic domains which form by the merger of these drops have a periodic distortion of the director field. Such configurations are not observed in usual nematics exhibited by pure compounds.

6.2 Experimental studies

The experiments have been performed on binary mixtures of a liquid crystalline compound and a polymeric 'impurity'. The liquid crystalline compound used in the experiments is trans-4-heptyl-(4-cyanopheny1)-cyclohexane $(PCH7)$. It has the following phase sequence as a function of temperature: isotropic – nematic – crystal. The isotropic to nematic transition occurs at 56.5^oC and the nematic phase extends down to room temperature. The molecular structure of this compound is shown below.

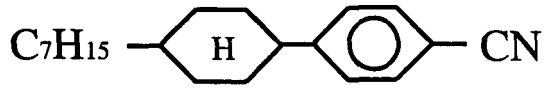

Figure 6.2: Molecular structure of the compound $PCH7$.

We have used two different commercially available polymeric materials in our studies. These are materials used in two-component adhesives and their chemical structures/compositions are not available. The polymers used do not have any liquid crystalline phases and are isotropic at room temperature $(\sim 25^oC)$. The results obtained with both the polymers are qualitatively the same. All the results presented here are from mixtures of $PCH7$ and one of the components of a commercial glue made by Lixon.

6.2.1 Sample preparation

The experiments were conducted on mixtures with about $18wt\%$ of the polymer. The required amount of each component was weighed into a small glass sample cup.

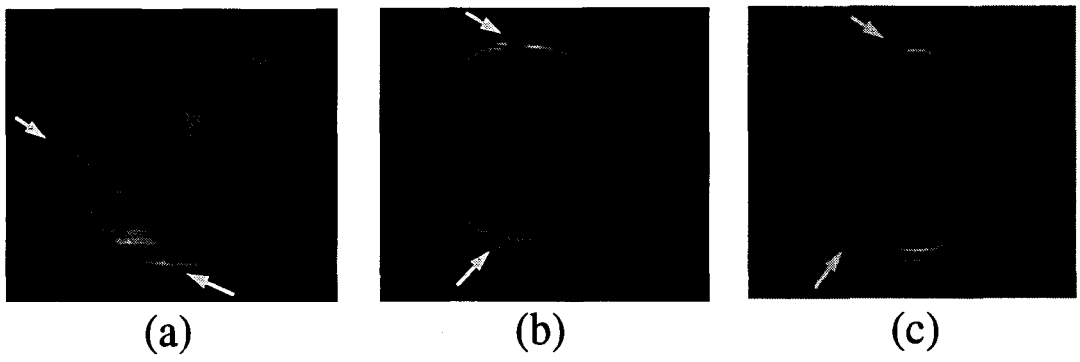

Figure **6.3:** Photographs of two disc-shaped drops (a),(b) taken between crossed polarisers which were along the horizontal and the vertical directions with respect to the pictures and (c) the second drop taken without one of the polarisers. The arrows show the positions of the two point disclinations which occur close together compared to the usual bipolar structure. The diameter of the drops are of the order of $200\mu m$.

The mixture was heated to the isotropic phase and mixed thoroughly before being filled into the sample cells. The polymer was completely miscible with PCH7 in the isotropic phase. The sample cells were constructed using clean glass plates. For this, the plates were first left in chromic acid for about an hour. The acid was removed by washing first with a mild detergent solution, then with distilled water and then with ethanol. The plates were then dried in an oven. The spacing between the glass plates was fixed using $50\mu m$ mylar spacers and the two plates were held together using an adhesive which does not mix with the sample. The cell thickness was measured from the interference pattern formed by white light reflected from the air film inside the cell using a constant deviation spectrometer (Adam and Hilger Ltd.). The cells were filled with the sample in the isotropic phase.

6.2.2 Microscopic observations

The sample temperature was controlled to an accuracy of $\pm O.l^{\circ}C$ using a Mettler $FP80$ hot-stage. The microscopic observations were made using a Leitz polarising microscope at x 250 magnification.

In the experiment, the sample was first heated to the isotropic phase and left

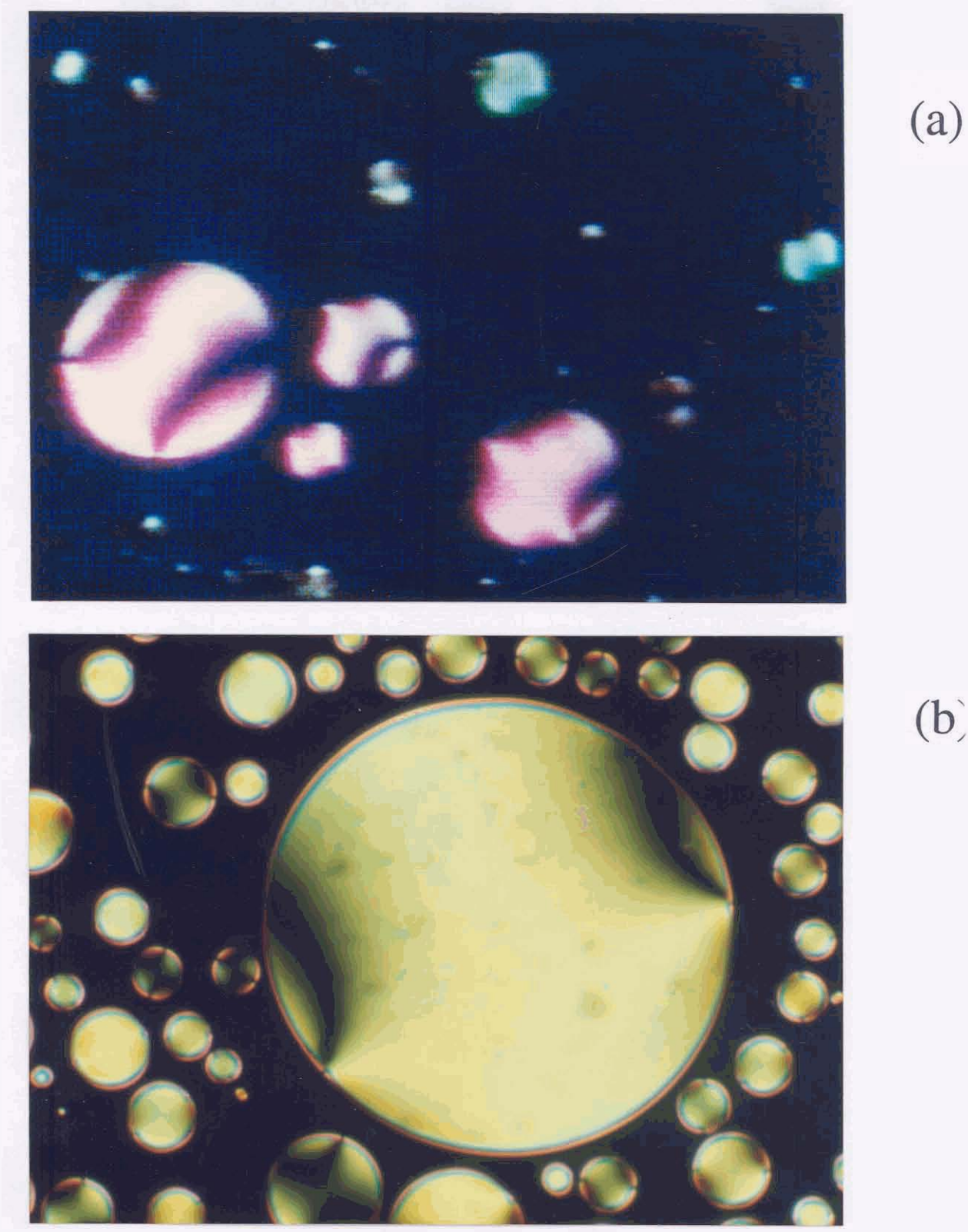

Figure 6.4: Photographs of two disc-shaped drops taken between crossed polarisers which were roughly along the horizontal and the vertical directions with respect to the pictures. The upper photograph (a) is grainy because it was taken from a video monitor. In the case of (b) the polymer concentration was low and hence the two defects are not very close to each other.

at a constant temperature for several minutes. This allowed it to attain a uniform concentration. It was then cooled at a rate of $0.1^{o}/min$. The isotropic to nematic transition started at $\sim 35^{o}C$. The nematic always nucleated in the bulk of the sample as tiny droplets. The droplets whose sizes were smaller than the cell thickness appeared spherical and had a bipolar configuration. The bipolar configuration indicates that the director at the NI interface prefers to lie in the local tangent plane. As the temperature was reduced, the drops grew in size. When the diameter of the drops became larger than the cell thickness, the growth was confined to the plane of the cell. This resulted in disc shaped drops. In such drops, the two point defects occurred closer together instead of being diametrically opposite to each other. Photographs of such drops taken between crossed polarisers are shown in Figs. 6.3a,b and Figs. 6.4a,b. The dark 'brushes' originating from the defects indicate regions where the director is either parallel or perpendicular to the polariser. Within the drops the director variation was smooth except near the defect cores. When the temperature was held constant, the structure remained unchanged for hours. The glass plates did not have any influence on the orientation of the director at the flat surfaces of the drops. This is because the polymeric material has a strong affinity for glass and hence a thin isotropic layer rich in the polymer forms near the two glass surfaces of the cell. This is easily verified by coating the glass surface with a layer of silicon monoxide at oblique incidence. Such a treatment favours a uniform alignment of the nematic director near the surfaces [30]. But in cells constructed using such treated glass plates no aligning effect was seen. This is because the isotropic layer prevents the nematic from coming into direct contact with the treated surfaces. Since the drops were in contact with an isotropic layer at the top and bottom surfaces, the director had a preference to lie in the plane of the interface and no particular azimuthal direction was preferred. The fact that the director was almost everywhere (except near the defects) in planes orthogonal to the viewing direction

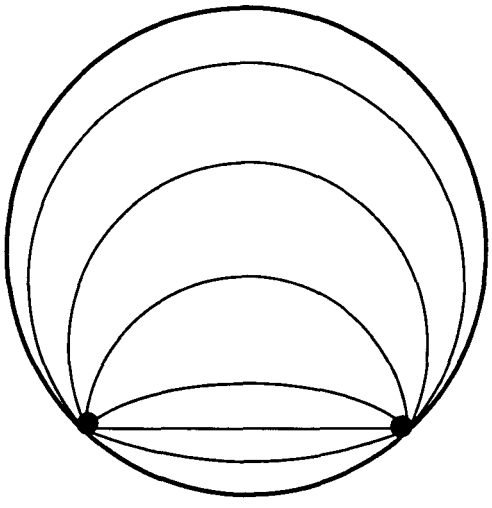

Figure 6.5: Schematic diagram of the director configuration within the disc-shaped drop.

---

made the the mapping of the director field quite easy.

Mapping the director field using crossed polariser and analyser will not give a unique director field. This is because the transmitted intensity is the same for director orientations which are locally rotated by $\pi/2$ at all points. Therefore, the director configurations within these drops were determined by doping the sample with a small amount of an azo dye.

The dye molecules are geometrically anisotropic and align along the nematic director. Moreover, the absorption is maximum when the electric-vector of the incident polarised light is parallel to the long axis of the dye molecule. Thus, by varying the polarisation direction of the incident light and noting the orientation of the polariser for maximum absorption for a given point in the drop, the director configuration can be mapped without any ambiguity.

The director configuration in the drops is shown in Fig. 6.5. Along the circumference of the disc the director is parallel to the local tangent to the circle. In the bulk, as well as at the top and bottom surfaces the director is parallel to the glass plates. The isotropic layers near the glass surfaces provide a free boundary where

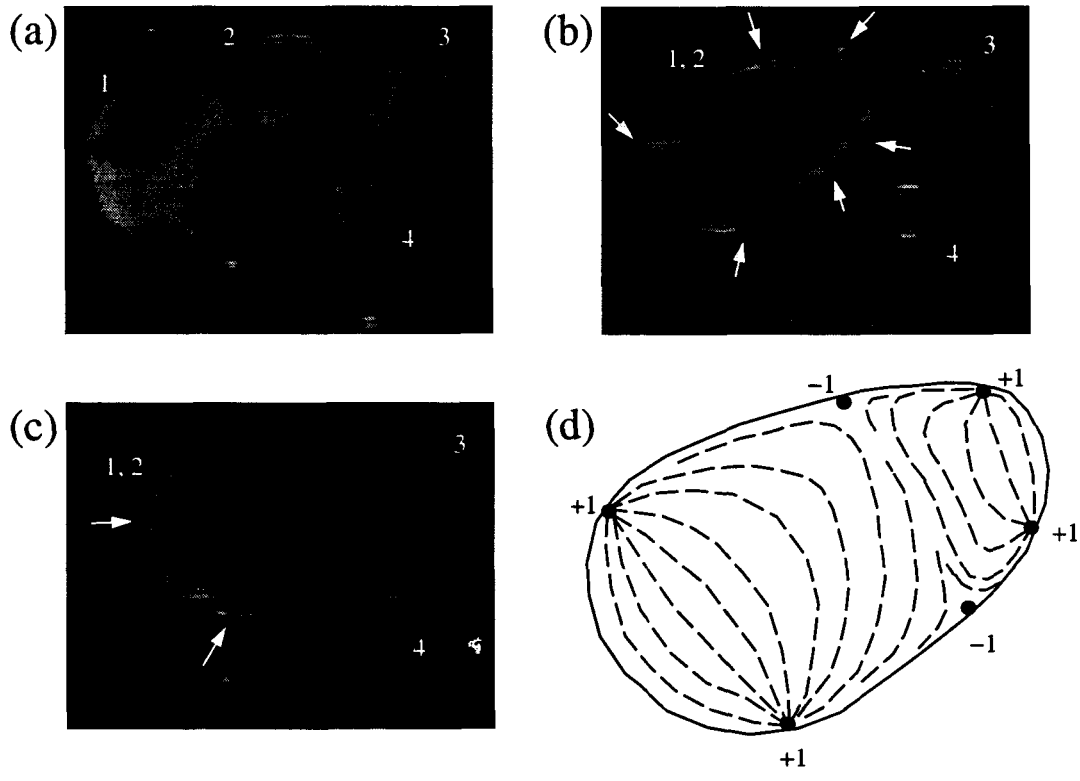

Figure 6.6: Sequence of photographs showing the coalescence of two bipolar drops. Two −1 defects are generated during this process which then cancels with two of the four +1 defects. The director field in (b) is schematically shown in (d).

the anchoring energy is degenerate with respect to the orientation of the director in the plane of the interface.

When the temperature was lowered further, the drops started merging and formed larger and larger domains. The configuration of the defects in these larger domains **was** very unusual. When two bipolar drops touch each other two negative surface disclinations are generated where the nematic-isotropic interfaces of the two drops meet. In usual bipolar drops, the two negative defects attract and cancel two of the total of four +1 defects. Thus, the resulting drop is left with two +1 defects and the net strength is again **+2.** In the case of the flattened drops, however, the extra pairs of defects generated during coalescence did not always cancel. **A** series of photographs showing the merger of two drops is shown in Fig. 6.6. In this case each negative defect was close to a positive defect and hence the two pairs could easily

cancel (Fig. 6.6b,c). The director distribution corresponding to Fig. 6.6b is shown in Fig. 6.6d. The structure of the resultant drop seemed to depend on the relative orientations of the two coalescing drops. When the drops merged in such a way that the positive defects in them were very close to the negative defects generated during merger, the extra pairs easily cancelled. On the other hand, when the drops merged with their defects on the same side of the line connecting the centers of the drops, one of the negative defects was far away from the positive ones. In such cases the isolated negative defect did not cancel with any of the positive ones. Two such possible scenarios are schematically shown in Figs. 6.7 and 6.8.

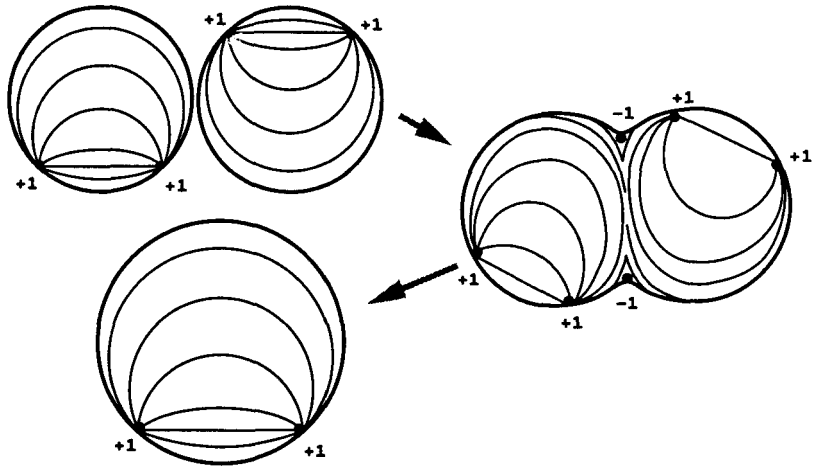

Figure 6.7: Schematic diagrams showing the coalescence of two disc-shaped drops with their defects on opposite sides of the line connecting their centers. The negative defects generated occur close to the positive ones and the pairs cancel easily as in usual bipolar drops.

Thus, when drops merged in this configuration, the resulting drop had an extra pair of defects. The net strength of $+2$ was, however, conserved. When many such drops merged the resulting domain had a large number of extra defect pairs. These pairs were arranged such that all the negative defects were on one side and the positive defects on the other. Photographs of the periodic patterns formed in this manner are shown in Figs. 6.9, 6.10 and 6.11. The director field had a periodic

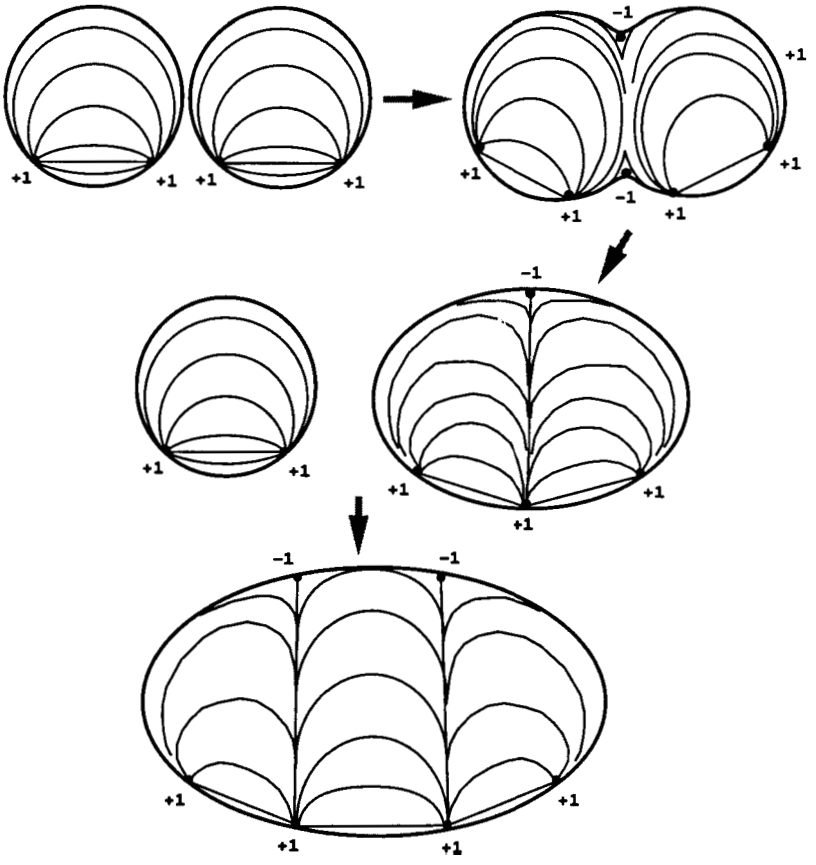

Figure 6.8: In this case the defects are on the same side of the line connecting the centers of the drops. When drops merge in this configuration, one negative defect is isolated from the positive ones and hence is not easily cancelled. Extra pairs of defects are generated when more drops merge in a similar configuration. The net strength in the resultant domains is always **+2.**

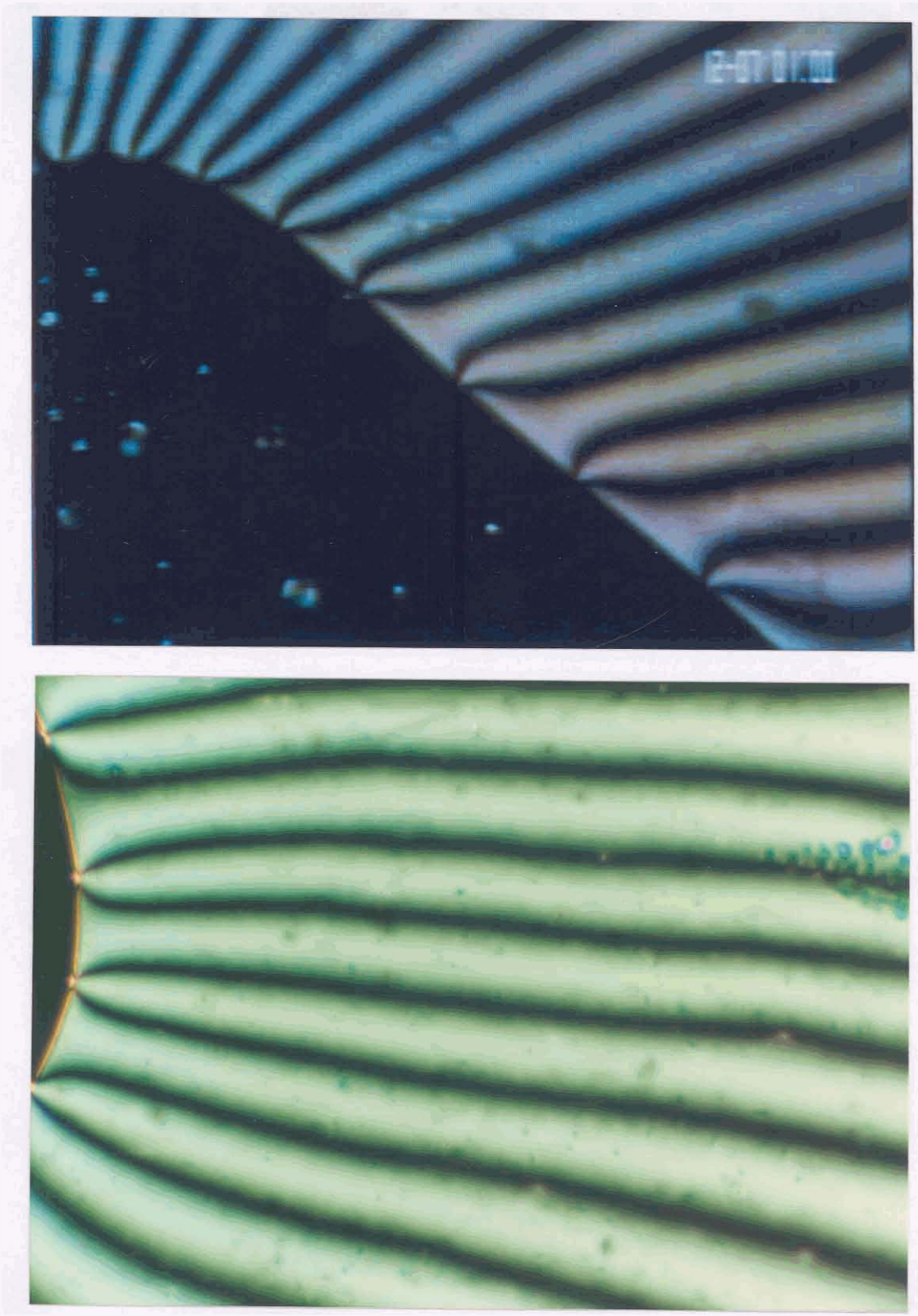

Figure 6.9: Stripped patterns formed by the merger of several bipolar drops, seen between crossed polarisers. The dark region is isotropic. The 'brushes' originate from surface disclinations which are arranged periodically at the interface. The periodicity is of the order of 200μm.

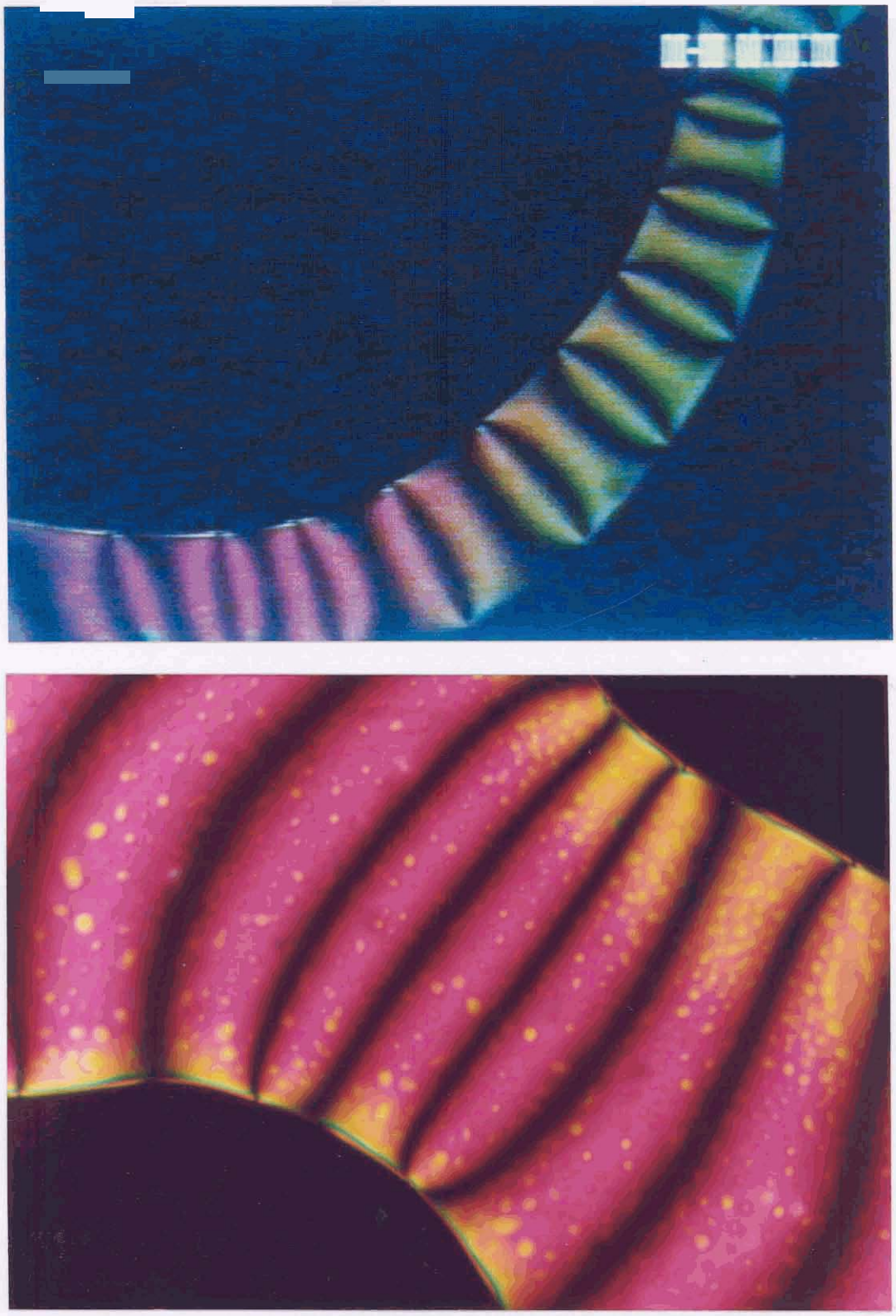

Figure 6.10: Periodic patterns seen in nematic strips bounded by the isotropic phase on both sides.

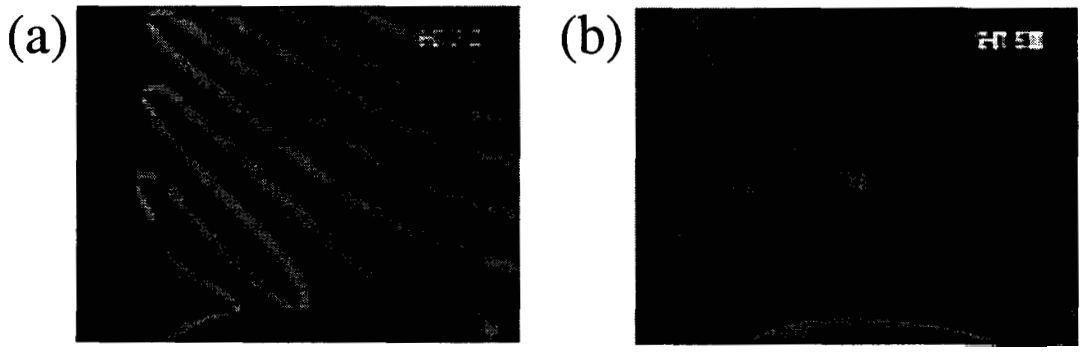

Figure 6.11: Pattern formed by a sample with a small amount of dye, recorded (a) between crossed polarisers and (b) without the analyser. The period was roughly of the order of $200\mu m$.

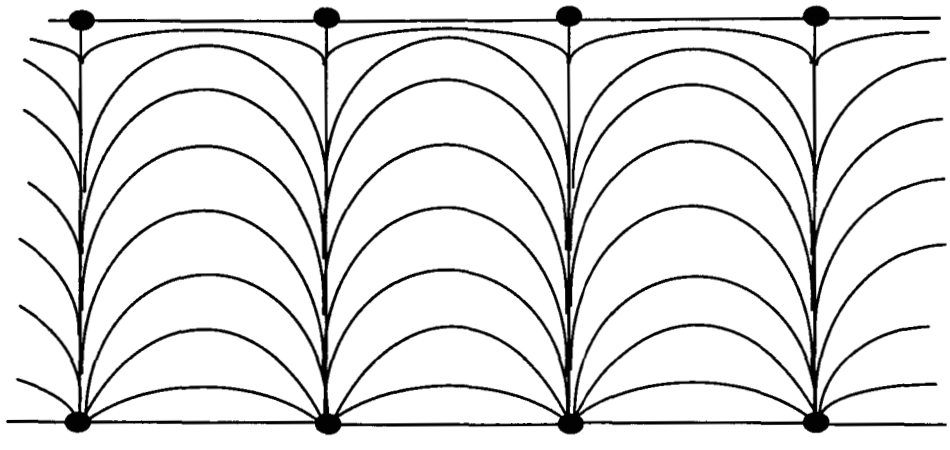

Figure 6.12: Schematic diagram of the director field that produces the periodic stripe pattern in a nematic 'slab' bounded by the isotropic phase. The surface disclinations at the upper interface are -1's and those at the lower boundary are $+1$'s.

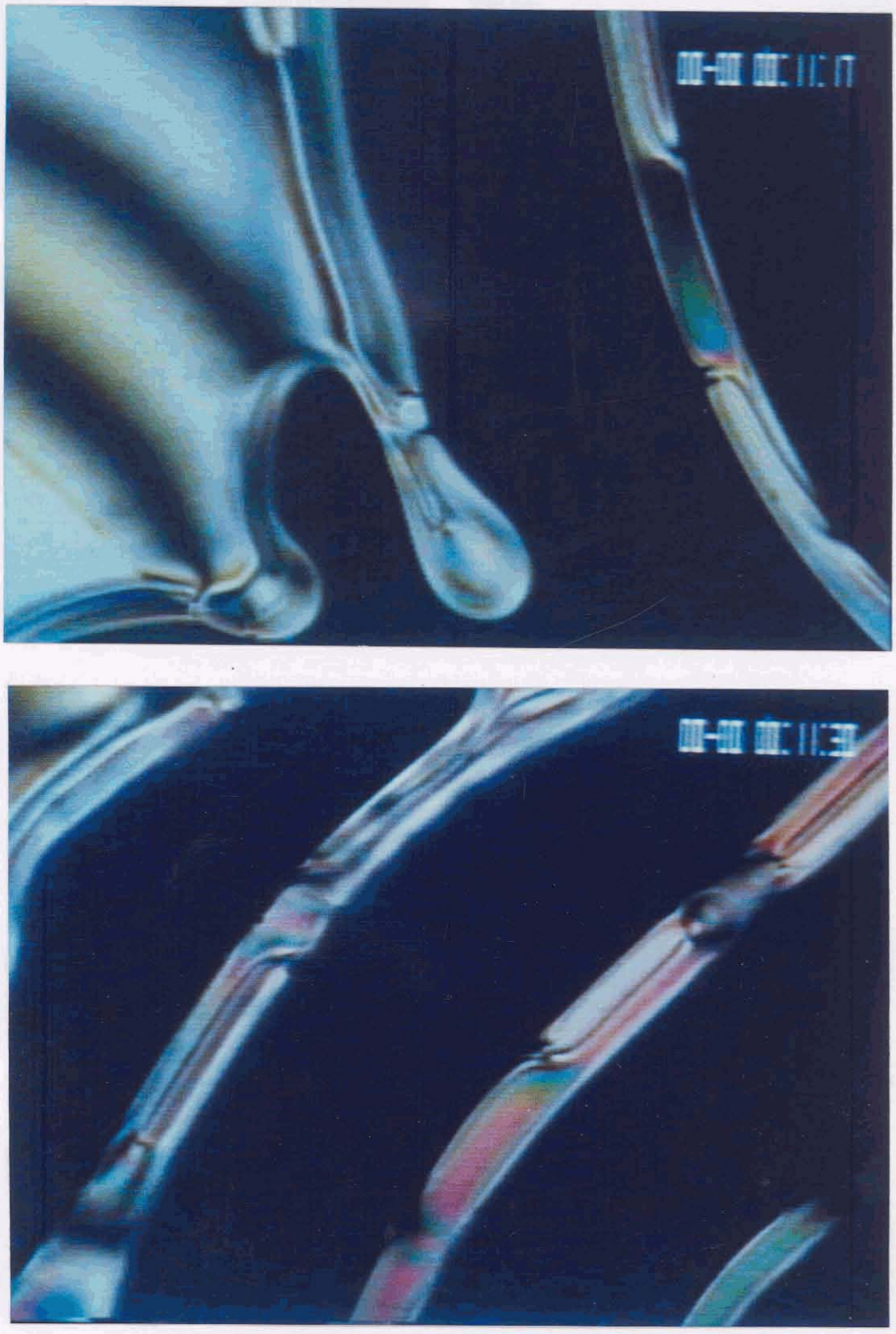

Figure 6.13: Sequence of photographs taken between crossed polarisers during fast heating. The isotropic phase forms channels which are roughly parallel to the stripes.

distortion as shown in Fig. 6.12. This periodic structure remained stable for hours.

When the sample was heated at a fast rate ($\sim 5^o/min$), the isotropic phase started nucleating at the defects and formed channels parallel to the stripes. The channels formed along the regions of maximum splay deformation. Since the transition temperature is lower when the polymer concentration is higher, this experiment clearly showed that there was a periodic variation in the concentration of the polymer which was coupled to the director field. This observation motivated us to analyse the effect of such a coupling in stabilising the new drop structure.

6.3 Theoretical analysis

In the case of the disc shaped drops, the director is parallel to the plane of the cell except very close to the defect-cores. Since the diameters of the drops were very much larger than the cell thickness, it is reasonable to assume that the director is everywhere parallel to the plane of the cell. Moreover, the director is uniform along the Z-axis which is taken to be normal to the disc. Thus, the director distribution can be described as

$$\hat{\mathbf{n}}(x, y) \equiv (n_x, n_y, 0) \; . \tag{6.2}$$

This implies that $\hat{\mathbf{n}} \cdot (\nabla \times \hat{\mathbf{n}}) = 0$, ie., there is no twist deformation. The Frank free energy density expression, **Eq.** 6.1, can then be written in the simple form

$$f_N = \frac{1}{2}\left[K_{11}(\nabla \cdot \hat{\mathbf{n}})^2 + K_{33}(\nabla \times \hat{\mathbf{n}})^2\right] \; . \tag{6.3}$$

From the experiments described earlier, it is clear that the concentration field is coupled to the director distortions. The concentration of the polymer is large close to the defects where the distortions are large. To the lowest order, the terms contributing to the energy density due to the coupling between the gradients in the concentration and the director distortions can be expressed as [71]

$$f_c = \nabla\chi \cdot \{a_1\hat{\mathbf{n}}(\nabla \cdot \hat{\mathbf{n}}) + a_3\,[\hat{\mathbf{n}} \times (\nabla \times \hat{\mathbf{n}})]\} + \frac{b}{2}(\nabla\chi)^2 \; , \tag{6.4}$$

where χ is the concentration of the polymeric impurity. The terms with coefficients a_1 and a_3 couple the concentration field to the splay and the bend distortions, respectively. These terms are allowed by the $\hat{\mathbf{n}} \equiv -\mathbf{ii}$ symmetry of the nematic medium. This coupling is analogous to the coupling between the flexoelectric polarisation and an external electric field [1]. The last term which is proportional to $(\nabla\chi)^2$ is required for stability of the uniform nematic. The total free energy density is given by

$$f = f_N + f_c \tag{6.5}$$

The total bulk energy is given by

$$F = \int d^3x\, f \,. \tag{6.6}$$

Minimising Eq.6.6 with respect to χ and integrating out the concentration field gives

$$F = \frac{1}{2}\int d^3x \left[\left(K_{11} - a_1^2/b\right)(\nabla\cdot\hat{\mathbf{n}})^2 + \left(K_{33} - a_3^2/b\right)(\nabla\times\hat{\mathbf{n}})^2\right] \,. \tag{6.7}$$

From Eqs. 6.3 and 6.7, we see that the effect of a non-zero impurity concentration is to renormalise the elastic constants of the pure nematic. Since b has to be positive for stability reasons, the effective elastic constants are lower compared to that of the pure nematic. The two coefficients, a_1 and a_3, can be very different when the nematic is doped with a polymer. This can lead to very large anisotropy in the elastic constants. We explored the possible role of such a large elastic anisotropy in stabilising the experimentally observed director configuration. The details of this calculation is described in the next section.

6.3.1 Calculations and results

From the Euler-Lagrange minimisation condition, we can define a 'molecular field' h [1], corresponding to a deformed director configuration, whose components are

$$h_i = \frac{\partial f}{\partial n_i} - \sum_j \frac{\partial}{\partial x_j}\left(\frac{\partial f}{\partial n_{ij}}\right) \,, \quad n_{ij} = \frac{\partial n_i}{\partial x_j} \,. \tag{6.8}$$

In equilibrium, the local director must be parallel to the molecular field at all points. Any deviation from this will produce a restoring elastic torque on the director. The local torque τ acting on the director is given by the relation

$$\tau = \hat{\mathbf{n}} \times \mathbf{h} \, . \tag{6.9}$$

Equilibrium is achieved when the torque acting on the director goes to zero at all points within the drop.

Since the director is confined to planes parallel to the XY-plane, it can be parameterised by an angle θ as

$$\hat{\mathbf{n}} \equiv (\cos\theta, \sin\theta, 0) \tag{6.10}$$

The torque balance equation, $\tau = 0$, can then be obtained as

$$\begin{aligned} (K_{11}\sin^2\theta + K_{33}\cos^2\theta)\,\frac{\partial^2\theta}{\partial x^2} + (K_{11}\cos^2\theta + K_{33}\sin^2\theta)\,\frac{\partial^2\theta}{\partial y^2} \\ + \frac{(K_{33}-K_{11})}{2}\sin(2\theta)\left[\left(\frac{\partial\theta}{\partial x}\right)^2 + \left(\frac{\partial\theta}{\partial y}\right)^2 + \frac{\partial^2\theta}{\partial x\partial y}\right] \\ + (K_{33}-K_{11})\cos(2\theta)\,\frac{\partial\theta}{\partial x}\frac{\partial\theta}{\partial y} \;=\; 0\,, \end{aligned} \tag{6.11}$$

Due to its highly non-linear nature, the torque balance equation, Eq.6.11, had to be solved numerically. This was done using the Successive Over Relaxation (SOR) method with Chebyshev acceleration [39].

The numerical minimisation was performed using a discretised version of the torque balance equation (6.11). For this the drop was divided into square cells of size a. Corrections are made on each cell, labeled by the indices i and j, according to the algorithm

$$\theta_{ij}^{new} = \theta_{ij}^{old} - \omega\frac{\tau_{ij}}{c_{ij}}\,, \tag{6.12}$$

where

$$c_{ij} = -\frac{1}{a^2}\left[2(K_{11}+K_{33}) + (K_{11}-K_{33})\sin(2\theta_{ij})\right] \tag{6.13}$$

[39] and w is the overrelaxation parameter. The optimum value for w was chosen empirically. The maximum mesh size that could be used was 200 x 200. The director configuration was always symmetric about a plane bisecting the line joining the two defects. This symmetry was exploited and only one half of the drop was simulated using the available mesh points.

In the calculation we started with a configuration with the two defects at diametrically opposite ends. Then one of the defects was moved along the circumference in small steps. At each step the structure was allowed to 'relax', subject to the tangential boundary condition, till the torques at every point was below a specified tolerance.

The numerical calculations showed that both the average splay and the bend deformations, integrated over the area of the drop, increased as the two defects were moved closer together along the circumference of the drop. Thus, with the free energy expression given by Eq.6.7, the stable structure is one with the two defects diametrically opposite to each other.

It should be mentioned that the numerical calculations involved considerable complications. One difficulty is in performing the numerical calculation in presence of singularities. Even if one puts a reasonable cut-off around the singular points, the large gradients in the director field close to the defects make numerical calculations inaccurate for practical mesh sizes. Moreover, the approximation of the circular region with square cells make the edges of the drop jagged. This is reflected in the variation of the distortion energy as the defect is moved along the circumference of the drop. The complicated geometry'makes it difficult to choose a space varying mesh size such that the mesh is finer where the distortions are more. Due to these reasons, it is difficult to make any conclusive remark on the effect of the elastic anisotropy in stabilising the drop structure based on the above calculations.

6.4 Conclusion

We have studied a new drop structure and pattern formation in a nematic doped with a polymeric impurity. Experiments show that the polymer concentration is coupled to the director field of the nematic. A simple theoretical model which takes into account such a coupling between the gradients in the concentration field and the director distortions does not seem to explain the experimental results. Therefore, other physical mechanisms have to be explored to understand these unusual patterns.

References

[1] P. G. de Gennes and J. Prost, The Physics of Liquid Crystals, 2nd ed. (Clarendon Press Oxford, 1993).

[2] S. Chandrasekhar, Liquid Crystals, 2nd ed. (Cambridge University Press, 1992).

[3] G. Vertogen and W. H. de Jeu, Thermotropic Liquid Crystals, Fundamentals (Springer-Verlag, 1988).

[4] S. Chandrasekhar, B. K. Sadashiva, and K. A. Suresh, Pramana 9, 471 (1977).

[5] R. B. Meyer et al., J. Phys. (Paris) Lett. **36,** L–69 (1975).

[6] P. M. Chaikin and T. C. Lubensky, Principles of condensed matter physics (Cambridge University Press, Great Britain, 1995).

[7] Kléman, Points Lines and Walls (John Wiley and Sons, 1983).

[8] S. R. Renn and T. C. Lubensky, Phys. Rev. A **38,** 2132 (1988).

[9] J. W. Goodby et al., Nature **337,** 449 (1989).

[10] P. G. de Gennes, Solid State Commun. **10,** 753 (1972).

[11] B. Pansu, M. H. Li, and H. T. Nguyen, Eur. Phys. J. B 2, 143 (1998).

[12] A. M. Levelut et al., J. Phys. II France 7, 981 (1997).

[13] L. Pasteur, C. R. Acad. Sci. Paris **26,** 535 (1848).

[14] D. K. Kondepudi, R. J. Kaufman, and N. Singh, Science **250,** 975 (1990).

[15] M. J. Press and A. S. Arrott, Phys. Rev. Lett. **33,** 403 (1974).

[16] J. B. Fournier and P. Galatola, J.Phys. 11 **5,** 1297 (1995).

[17] J. Pang and N. A. Clark, Phys. Rev. Lett. **73,** 2332 (1994).

[18] J. V. Selinger and R. L. B. Selinger, Phys. Rev. E **51,** R860 (1995).

[19] B. Martin, A. Tharrington, and X. 1. Wu, Phys. Rev. Lett. **77,** 2826 (1996).

[20] M. V. Kurik and O. D. Lavrentovich, Sov. Phys. Usp. **31,** 196 (1988).

[21] J. Maclennan and M. Seul, Phys. Rev. Lett. **69,** 2082 (1992).

[22] J. V. Selinger, Z.-G. Wang, R. F. Bruinsma, and C. M. Knobler, Phys. Rev. Lett. **70,** 1139 (1993).

[23] L. Bourdon, J. Sommeria, and M. Kléman, J. Physique **43,** 77 (1982).

[24] R. Pratibha and N. V. Madhusudana, J. Phys. II (France) **2,** 383 (1992).

[25] M. V. Kurik and O. D. Lavrentovich, Sov. Phys. JETP **58,** 299 (1983).

[26] D. Demus and L. Richter, *Textures* of *Liquid Crystals* (Verlag Chemie publications, 1978).

[27] J. B. Foumier and G. Durand, J. Phys. II (France) **1,** 845 (1991).

[28] G. W. Smith and Z. G. Gardlund, J. Chem. Phys. **59,** 3214 (1973).

[29] N. V. Madhusudana, K. P. L. Moodithaya, and K. A. Suresh, Mol.Cryst **99,** 239 (1983).

[30] W. Urbach, M. Boix, and E. Guyon, Appl. Phys. Lett. **25,** 479 (1974).

[31] S. A. Langer and J. P. Sethna, Phys. Rev. A **34,** 5035 (1986).

[32] N. V. Madhusudana and B. S. Srikanda, Mol. Cryst. Liq. Cryst. **99, 375 (1983).**

[33] P. E. Cladis and S.Torza, J. Appl. Phys. **46, 584 (1975).**

[34] Forgan, Cryogenics **14, 207 (1974).**

[35] F. M. Leslie, I. W. Stewart, and M. Nakagawa, Mol. Cryst. Liq. Cryst. **198, 443 (1991).**

[36] Lagerwall, S. **T.,** and I. Dahl, Mol. Cryst. Liquid. Cryst. **114, 151 (1984).**

[37] Orsay group on Liquid Crystals, Solid State Commun. **9, 653 (1971).**

[38] G. Barbero, I. Dozov, J. F. Palierne, and G. Durand, Phys. Rev. Lett. **56, 2056 (1986).**

[39] W. H. Press, S. A. Teukolsky, W. T. Vellerling, and B. P. Flannery, Numerical recipes, 2nd ed. (Cambridge university press, **1982).**

[40] A. Yariv, Optical Waves in Crystals (Wiley-Interscience Publication, **1983).**

[41] R. Ondris-Crawford, E. P. Boyko, B. G. Wagner, J. H. Erdmann, S. Zumer, and J. W. Doane, J. Appl. Phys. **69, 6380 (1991).**

[42] N. W. Ashcroft and N. D. Mermin, Solid State Physics, international edition ed. (Saunders College Publishing, **1976).**

[43] K. J. Ihn et al., Science **258, 275 (1992).**

[44] L. Navailles et al., Phys. Rev. Lett. **74, 5224 (1995).**

[45] S. R. Renn, Phys. Rev. **A 45, 953 (1992).**

[46] W. Kuczynski and H. Stegemeyer, Mol. Cryst. Liq. Cryst. **260, 377 (1995).**

[47] W. Kuczynski, SPIE **3318, 90 (1998)**

[48] Z. Raszewski *et* al., Ferroelectrics **147,** 281 (1993).

[49] Z. Raszewski *et* al., Mol. Cryst. Liq. Cryst. **263,** 271 (1995).

[50] G. Sprouce and R. D. Pringle, Liquid Crystals **3** No. **4,** 507 (1988).

[51] A. de Vries, Mol. Cryst. Liq. Cryst. **10, 11,** 31, 219, 361 (1970).

[52] J. W. Goodby *et* al., J. Am. Chem. Soc. **111,** 8119 (1989).

[53] N. L. Kramarenko *et* al., Liquid Crystals **22,** 535 (1997).

[54] T. Chan, C. W. Garland, and H. T. Nguyen, Phys. Rev. E 52, 5000 (1995).

[55] L. Navailles, C. W. Garland, and H. T. Nguyen, J. Phys. II France **6,** 1243 (1996).

[56] R. D. Kamien and T. C. Lubensky, J. Phys. I France **3,** 2131 (1993).

[57] N. Isaert *et* al., J.Phys.II France 4, 1501 (1994).

[58] B. Pansu, Private communication .

[59] P. E. Cladis, H. R. Brand, and P. L. Finn, Phys. Rev. A **28,** 512 (1983).

[60] P. Barois, Private communication .

[61] B. K. Sadhasiva, Private communication .

[62] S. R. Renn and T. C. Lubensky, Mol. Cryst. Liq. Cryst **209,** 349 (1991).

[63] I. Dozov, Phys. Rev. Lett. **74,** 4245 (1995).

[64] J. B. Fournier, I. Dozov, and G. Durand, Phys. Rev. A **41,** 2252 (1990).

[65] P. Galatola, J. B. Fournier, and G. Durand, Phys. Rev. Lett **73,** 2212 (1994).

[66] J. W. Goodby et al., *Ferroelectric Liquid* Crystals (Gordon and Breach Publishers, 1991).

[67] A. C. Ribeiro et al., Eur. Phys. J. B **1,** 503 (1998).

[68] G. E. Volovik and O. D. Lavrentovich, Sov. Phys. JETP **58,** 1159 (1983).

[69] A. V. Koval'chuk et al., Sov. Phys. JETP **67,** 1065 (1988)

[70] P. Drzaic, Mol. Cryst. Liq. Cryst. **154,** 289 (1988)

[71] S. Ramaswamy et al., Mol. Cryst. Liq. Cryst. **288,** 175 (1996).